PCCP

ROYAL SOCIETY OF CHEMISTRY

PAPER

View Article Online
View Journal

Cite this: DOI: 10.1039/d1cp04539c

First-principles calculations on the resistance and electronic properties of H_2 adsorption on a CoO–SnO_2 heterojunction surface†

Yunxia He, [a] Jing Li,*[a] Lin Tao, *[b] Shuai Nie,[a] Timing Fang,[c] Xitao Yin [d] and Qi Wang[a]

Compared with pure metal oxides, heterojunctions greatly change the response to gas by the synergistic effect of the interface. In this work, density functional theory was used to reveal the adsorption performance of H_2 on the heterojunction under oxygen conditions. First, we determined the most reasonable heterojunction structure based on the adhesion work. According to the adsorption energy, the presence of SnO_2(100)(I)/CoO(110)(II) made the adsorption of H_2 more stable. The DOS results showed that the resistance of the heterojunction increased with H_2 adsorption, following the same trend as that of CoO(110) with H_2 adsorption, although that of the heterojunction increased more. The electron density and electron density difference indicated that the heterojunction improved the reaction between H_2 and oxygen ions on CoO(110). However, the resistance of CoO(110)(II)/SnO_2(100)(II) increased after H_2 adsorption, contrary to the resistance change of SnO_2(100). Besides, the bonding energy between H_2 and the adsorption site became worse. The above results demonstrated that the presence of the heterojunction could indeed change the response trend and the adsorption behavior of H_2. Interestingly, the adsorption sites and effects of H_2 were different when two metal oxides were used as the substrate of the heterojunction, respectively.

Received 4th October 2021,
Accepted 15th November 2021

DOI: 10.1039/d1cp04539c

rsc.li/pccp

1. Introduction

Semiconductor metal oxides as a material for chemical gas sensors play a significant role thanks to their abundance, low cost, and easy manufacture. Among these semiconductor metal oxide gas sensors, compounds made of adsorbed air oxygen ions and the target gas on the surface cause a change in the electric resistance of the materials. These semiconductor metal oxide gas devices have sensitivity to various toxic, flammable, and explosive gases, and are widely applied in various fields.[1–4]

However, metal oxide gas devices suffer from the effects of baseline resistance drift and from poisoning interactions. These problems make it progressively more and more difficult for metal oxide surfaces to approach reactive gases.[5,6] SnO_2 semiconductors are among the best n-type metal oxide gas-sensing materials for gas-sensitive devices owing to their wide band gap, excellent chemical stability, and prominent sensitivity.[7] However in practical applications, the gas sensitivity to H_2 still needs to be improved for the accurate identification of H_2. Surface modification[8–10] is the most commonly used approach to enhance the H_2 sensitivity.[11] However, the response effect is not obvious. Decorating H_2-response sieves[12–15] and polymers[16] on the surface of gas-sensing materials has also been explored to enhance H_2 sensitivity. These are new innovation, but the accurate identification for H_2 needs to be improved. In addition, as one p-type metal oxide gas-sensing material, CoO has shown an affinity with oxygen and possesses multivalent characteristics.[17] The pristine form of CoO is hardly used in the field of sensing due to its lower response than n-type semiconductors,[18] though it has been reported that its gas-sensing can be significantly improved by introducing dopants,[19] or by proper control of the morphology.[20,21] However, the accurate identification of gases still needs to be improved.

The idea of combining different metal oxide materials to form a heterojunction was recently proposed in order to further improve the important sensing characteristics of resistive-type gas sensors.[22,23] Generally, n-type materials have a higher

[a] School of Materials and Metallurgy, University of Science and Technology Liaoning, Anshan 114051, Liaoning, China. E-mail: lijing_as321@163.com
[b] School of Chemical Engineering, University of Science and Technology Liaoning, Anshan 114051, Liaoning, China. E-mail: taolin_phd@163.com
[c] School of Chemistry and Chemical Engineering, Qingdao University, Qingdao 266071, Shandong, China
[d] School of Physics and Optoelectronic Engineering, Ludong University, Yantai 264000, Shandong, China

† Electronic supplementary information (ESI) available. See DOI: 10.1039/d1cp04539c

Fermi energy level than that of p-type materials.[24] Hence, when n-type and p-type heterojunctions are fabricated, the electrons of n-type metal oxides with a higher energy will pass through the interface to the vacant lower-energy states until the Fermi energy level achieves a stable condition. The potential barrier, which is attributed to the difference in Fermi energy levels, will show an obvious change when a heterojunction is surrounded by different oxidizing or reducing gases. Furthermore, the changes will be observed as a high response in composite heterojunction gas sensors.[25] The synthesis of a heterojunction provides a significant method to incorporate different physical and chemical properties into one system.[26]

A large number of studies have applied first-principle calculations on the various properties of heterojunctions,[27–30] and extensive research studies on the formation of heterojunctions have been published. Katoch *et al.*[31] researched an n-p ZnO/CuO heterojunction as s nanofiber sensor to strengthen the primary ZnO nanofiber sensor sensing in H_2S. Similarly, Choi *et al.*[32] reported the gas-sensing of H_2S was boosted in a CuO/SnO_2 heterojunction more than in the bulk of SnO_2 owing to the formation and disruption of the heterojunction. Ju *et al.*[33] proved that a NiO/SnO_2 heterojunction had a more rapid response to trimethylamine than pure SnO_2. Other research into metal oxide p–n heterojunction NiO/ZnO,[34] NiO/Fe_2O_3,[35] and NiO/SnO_2[36] have experimentally proved that the formation of a metal oxide heterojunction would obviously strengthen a sensor's gas sensitivity. The performances of metal oxide of Sn and Co can also be improved greatly by forming a p–n heterojunction.[37,38] Heterojunctions have been applied to strengthen the sensing properties of sensors based on SnO_2 through altering the influence at the synthesis interface.

However, explanations about the microstructure and theories about the mechanism of heterojunctions are obscure. Not only does this show a misfit, but also the structure and adhesion strength of the interface affect the effectiveness of promoting heterogeneous nucleation.[39,40] It is very difficult to observe structures and the adhesion strength of an interface or the adsorption of H_2 on a heterojunction surface through experimental methods. In this respect, an atomic level understanding about the H_2-sensing mechanism on SnO_2–CoO materials is crucial. Meanwhile, the gas-sensing characteristics, such as adsorption performance of metal oxide sensors, should be visualized for practical application.[41] First-principles calculations have been employed to reveal the structures and adhesion strength of the interface at the atomic scale,[42–45] and the adsorption of gases on a single metal oxide calculated,[46–51] including the adsorption energy, adsorption distance, DOS, and electronic structure.

In this work, we studied the microstructure of SnO_2/CoO and CoO/SnO_2 heterojunctions by DFT, analyzing the transformation of the resistance, electronic structure, and other properties of H_2 adsorption on different sites of the heterojunction surface. Moreover, this work can provide theoretical guidance for the fabrication of heterojunction gas sensors in order to accurately identify H_2.

2. Methods

2.1 Calculation details

The Cambridge Serial Total Energy Package (CASTEP) Code was used for all the calculations based on density functional theory (DFT).[52–54] The Generalized Gradient Approximation (GGA) of the Perdew–Burke–Ernzerhof (PBE) scheme was employed to describe the exchange–correlation functional. Considering the stability of the system and for optimization of the calculation speed, the plane wave cut-of energy was selected as 400 eV. The Brillouin zone was sampled by $3 \times 3 \times 1$ *k*-points using the Monkhorst–Pack scheme. The convergence tolerance for the energy was selected as 2.0×10^{-6} eV per atom. The force, stress, and displacement tolerance of the convergence tolerance were set as 0.05 eV Å^{-1}, 0.1 GPa, and 0.002 Å, respectively. To avoid the interaction between surface atoms, a vacuum layer of 15 Å was selected for each heterojunction surface system.

2.2 CoO–SnO_2 heterojunction models

Chemiresistive gas sensors employing a p–n heterojunction offer a compelling high sensitivity and specific response.[55] The interfacial free energy between the precipitations and the substrates control the process of particle coarsening. Being based on the lattice mismatch theory,[56] the interface with the lowest lattice mismatch between the second particle and the pre-existing particle will be the preferred growth direction of the second particle on the pre-exiting particle.[57] The primitive cells made from the CoO(110) surface and SnO_2(100) surface possessed lattice constants of $a_{CoO(110)}$ = 4.2667 Å, $b_{CoO(110)}$ = 3.017013 Å, $a_{SnO_2(100)}$ = 4.73727 Å, $b_{SnO_2(100)}$ = 3.186383 Å. The mismatch between CoO(110) and SnO_2(100) was less than 6%. Therefore, SnO_2(100) and CoO(110) were selected to structure the heterojunction. As shown in Fig. 1(a and b), the surface termination of CoO(110) has two forms:[58–60] CoO(110)(I) (1O and 1/4Co as termination) and CoO(110)(II) (1O and 1/2Co as termination). In addition, the surface termination of SnO_2(100) has four different surface terminations: SnO_2(100)(I) (1/4Sn-termination), SnO_2(100)(II) (1/2O-termination), SnO_2(100)(III) (1Sn-termination), and SnO_2(100)(IV) (1O-termination), as

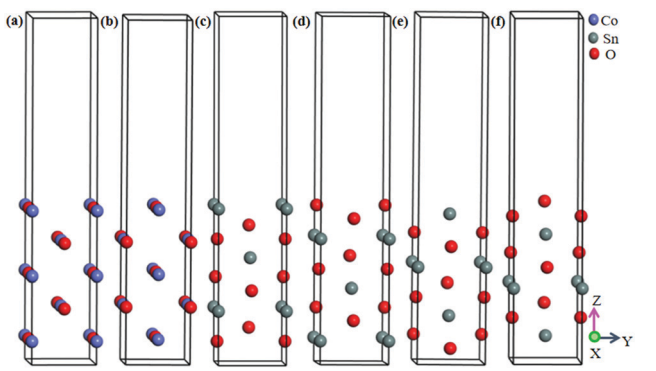

Fig. 1 Surface structure of CoO(110) and SnO_2(100). (a) CoO(110)(I), (b) CoO(110)(II), (c) SnO_2(100)(I), (d) SnO_2(100)(II), (e) SnO_2(100)(III), (f) SnO_2(100)(IV).

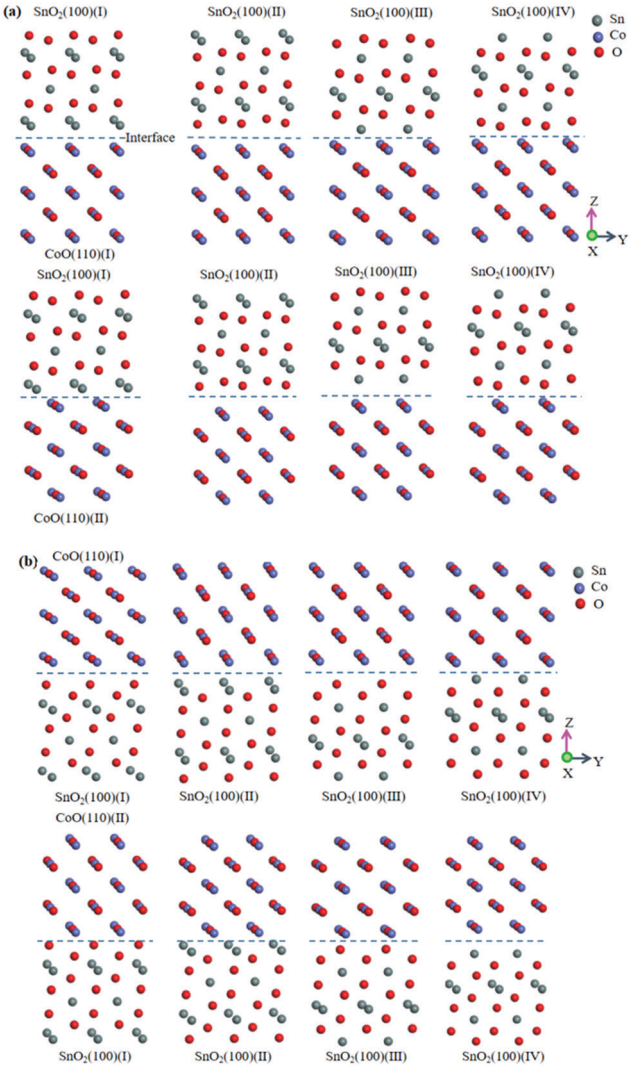

Fig. 2 Different models of CoO/SnO_2 heterojunction and SnO_2/CoO heterojunction. (a) SnO_2(100) was put on CoO(110); (b) CoO(110) was put on SnO_2(100).

shown in Fig. 1(c–f). There are sixteen kinds of heterojunction due to the four terminations of SnO_2(100) and two terminations of CoO(110), which are shown in Fig. 2(a) and (b). In order to reduce the effect of lattice interactions on the adsorption, (1 × 2) supercellular SnO_2(100)–CoO(110) heterojunctions were fabricated.

3. Results and discussion

3.1 Adsorption properties of H_2 on the heterojunction surface

3.1.1 Adhesion work of the heterojunction. The adhesion work (W_{ad}) needed to be calculated, in order to gain an insight into the binding strength of the interface, where W_{ad} is defined as the reversible work of separating the interface into two free surfaces, and is given by the difference in the total energy between the interfaces. Generally, a larger W_{ad} is associated with a more stable interface. The adhesion work is defined as follows:[61–63]

$$W_{ad} = \frac{(E_{CoO} + E_{SnO_2} - E_{SnO_2/CoO})}{A} \quad (1)$$

where E_{SnO_2} and E_{CoO} are the total energy of SnO_2 and CoO slabs, respectively, $E_{SnO_2/CoO}$ represents the total energy of the heterojunction interface, and A is the interface area.

The interfaces of the SnO_2(100)/CoO(110) system and CoO(110)/SnO_2(100) system showed the same distances (2 Å), which were optimized by energy calculation for evaluating the interface properties of the heterojunction. The interface structures were optimized with in a fixed cell volume, and all the atoms at the interface models were allowed to relax in three directions.[64] The W_{ad} values of the heterojunction are shown in Table 1.

Table 1 Bonding energy (J m^{-2}) of SnO_2–CoO heterojunctions

Heterojunction	W_{ad} (J m^{-2})
SnO_2(100)(I)/CoO(110)(I)	−0.5179
SnO_2(100)(II)/CoO(110)(I)	−0.5187
SnO_2(100)(III)/CoO(110)(I)	−0.5203
SnO_2(100)(IV)/CoO(110)(I)	−0.5194
SnO_2(100)(I)/CoO(110)(II)	−0.5175
SnO_2(100)(II)/CoO(110)(II)	−0.5191
SnO_2(100)(III)/CoO(110)(II)	−0.5177
SnO_2(100)(IV)/CoO(110)(II)	−0.5191
CoO(110)(I)/SnO_2(100)(I)	−0.5189
CoO(110)(I)/SnO_2(100)(II)	−0.5185
CoO(110)(I)/SnO_2(100)(III)	−0.5195
CoO(110)(I)/SnO_2(100)(IV)	−0.5176
CoO(110)(II)/SnO_2(100)(I)	−0.5176
CoO(110)(II)/SnO_2(100)(II)	−0.5175
CoO(110)(II)/SnO_2(100)(III)	−0.5195
CoO(110)(II)/SnO_2(100)(IV)	−0.5182

Table 1 shows the adhesion work of the SnO_2(100)/CoO(110) heterojunctions, where it can be seen that the adhesion work of the SnO_2(100)(I)/CoO(110)(I) and SnO_2(100)(I)/CoO(110)(II) heterojunctions were larger than that of the other heterojunctions. Therefore, they were more stable than the other SnO_2(100)/CoO(110) heterojunctions. However, SnO_2(100)(I)/CoO(110)(II) heterojunction had a larger W_{ad} than that of the SnO_2(100)(I)/CoO(110)(I) heterojunction. Therefore, the SnO_2(100)(I)/CoO(110)(II) heterojunction was selected as the adsorption carrier of H_2, which was attributed to its larger adhesion work.

Table 1 shows the adhesion work of the CoO(110)/SnO_2(100) heterojunctions. It shows that the W_{ad} values of the CoO(110)(II)/SnO_2(100)(I), CoO(110)(II)/SnO_2(100)(II), and CoO(110)(I)/SnO_2(100)(IV) heterojunctions were larger than those of the other CoO(110)/SnO_2(100) heterojunctions. Therefore, they were more stable than the other CoO(110)/SnO_2(100) heterojunctions. Although three heterojunctions had approximately the same W_{ad}, the CoO(110)(II)/SnO_2(100)(II) heterojunction had the larger W_{ad}. Consequently, the

CoO(110)(II)/SnO_2(100)(II) heterojunction system was chosen as the adsorption carrier of H_2.

3.1.2 Adsorption energy of H_2 on the heterojunction. In the air atmosphere, the oxygen in the air will capture the electrons on the surface of a heterojunction to form adsorbed oxygen anions.[66] Consequently, it was necessary to first find out the most stable adsorption site and configuration of O_2 molecule on the heterojunction surface. The adsorption behaviors of O_2 molecules on the heterojunction surface are shown in Fig. S1 and S2 (ESI†); in addition, the related parameters are shown in Tables S1 and S2 (ESI†). The results showed that different heterojunction terminals have different oxygen adsorption configurations. The most stable adsorption structure of O_2 on the heterojunction surface is shown in Fig. 3. Therefore, we used these structures as the initial configurations to explore the adsorption behavior of H_2 on the heterojunctions.

There were nine different types of adsorption conditions of H_2 on SnO_2(100)(I)/CoO(110)(II) and CoO(110)(II)/SnO_2(100)(II) heterojunctions in an oxygen atmosphere (including the adsorption on the O_2 molecule and different sites of the heterojunction surface), which are shown in Fig. 4(a–e) and (f–i).[67]

The adsorption energy (E_{ads}) is a key standard to estimate the adsorption property of H_2 molecules on the heterojunction surface. It can be adopted to judge the adsorption strength of H_2 molecules on a carrier, which is defined as follows:[68,69]

$$E_{ads} = E_{total} - (E_{heterojunction} + E_{gas}) \quad (2)$$

where E_{ads} is the adsorption energy (eV), E_{total} represents the total energy of the whole adsorption system, $E_{heterojunction}$ is the total free energy of the heterojunction system (eV), and E_{gas} is the total free energy of an isolated gas molecule (eV). In general, E_{ads} with a negative value indicates that the adsorption is exothermic, and the system of adsorption is energetically stable.[70,71]

The E_{ads} and the adsorbed distance of H_2 adsorption on the SnO_2(100)(I)/CoO(110)(II) and CoO(110)(II)/SnO_2(100)(II) heterojunctions are shown in Table 2. In addition, the parameters about E_{ads} and the adsorbed distance of H_2 on single material oxide CoO and SnO_2 are shown in Tables S3 and S4 (ESI†).

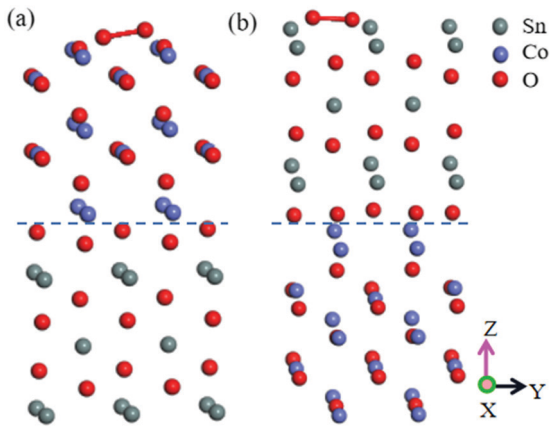

Fig. 3 The most stable adsorption structure of O_2 molecule on the heterojunction surface. (a) O_2 on the SnO_2(100)(I)/CoO(110)(II) heterojunction, (b) O_2 on the CoO(110)(II)/SnO_2(100)(II) heterojunction.

Table 2 shows the E_{ads} and adsorption distance when H_2 was adsorbed on different sites of the SnO_2(100)(I)/CoO(110)(II) heterojunction surface. There were five forms where H_2 was adsorbed on the heterojunction surface, including the O site of an O_2 molecule, and O1 site, O2 site, Co1 site, Co2 site of the heterojunction surface. The adsorption distance and E_{ads} varied greatly. When H_2 was adsorbed on the O site of an O_2 molecule, the distance of H–O bonding was less than 3 Å, indicating the formation of a chemical bond. Except at the Co2 site, the E_{ads} values were all negative when H_2 was adsorbed on other sites of the heterojunction surface. This reveals the preferable stabilization of adsorption, especially the adsorption on an O site of an O_2 molecule, and O1 site and O2 site of the heterojunction surface. Therefore, according to the W_{ads} and adsorption distance, it was easy for H_2 to be adsorbed on an O site of an O_2 molecule. Compared with pure metal oxides CoO, the SnO_2(100)(I)/CoO(110)(II) heterojunction improves the adsorption and bonding of H_2 on an O_2 molecule. Also, the adsorption of H_2 on the heterojunction was more stable.

Table 2 shows the E_{ads} and adsorbed distance of H_2 adsorption on O site of an O_2 molecule, Sn (Sn is equivalent because of supercell) site, and O1 site and O2 site of the CoO(110)(II)/SnO_2(100)(II) heterojunction surface. The adsorption distance and E_{ads} varied greatly. The adsorbed distances were all more than 3 Å when H_2 was adsorbed on different sites of the heterojunction surface. This implies the existence of weak chemical bonding between H atoms and the adsorbed sites. In addition, the E_{ads} values were obviously different when H_2 was adsorbed on different surface sites. The E_{ads} values were all negative when H_2 was adsorbed on the heterojunction surface, revealing that the adsorption of H_2 on the heterojunction was thermodynamically stable. Consequently, it was easy for H_2 to be adsorbed on the CoO(110)(II)/SnO_2(100)(II) heterojunction surface by analyzing the adsorbed distance and E_{ads}. However, there was no formation of stronger chemical bonding between H_2 molecules and the adsorbed sites. Compared with pure metal oxides SnO_2, the existence of the CoO(110)(II)/SnO_2(100)(II) heterojunction made the bonding effect between H_2 and adsorption sites worse, but made the adsorption more stable, especially the adsorption of H_2 on the O1 site.

In summary, based on the E_{ads} and adsorption distance, H_2 readily adsorbs on an O_2 molecule of the SnO_2(100)(I)/CoO(110)(II) heterojunction surface. In addition, H_2 tends to be adsorbed on different sites of the CoO(110)(II)/SnO_2(100)(II) heterojunction surface; however, stronger chemical bonds did not exist.

3.2 Influence of gas adsorption on the electronic conductivity and electronic structure

3.2.1 Density of states (DOS). To understand the adsorption effect of H_2 on the conductivity of a heterojunction in the oxygen atmosphere, DOS analysis was performed of single metal oxide CoO and SnO_2 adsorbed O_2 on surface. The adsorption of one O_2 molecule on the CoO and SnO_2 surface

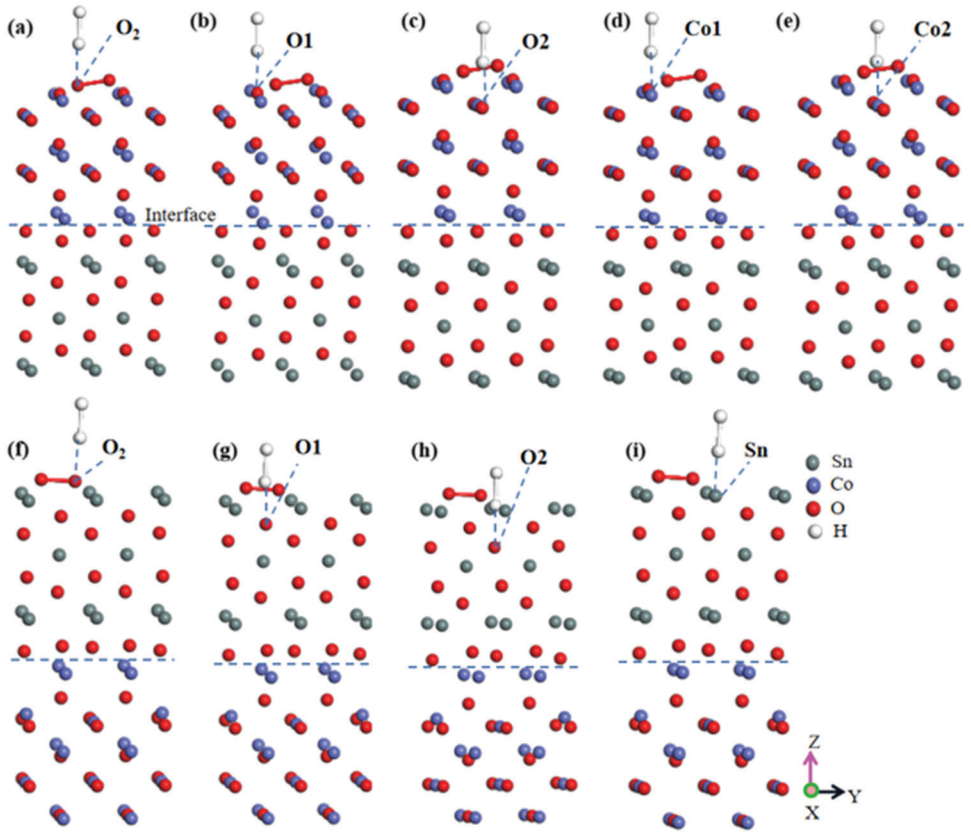

Fig. 4 H_2 adsorbed on different sites of heterojunction surfaces. (a–e) H_2 on the SnO_2(100)(I)/CoO(110)(II) heterojunction, (f–i) H_2 on the CoO(110)(II)/SnO_2(100)(II) heterojunction.

Table 2 Adsorption of H_2 on the heterojunctions

Heterojunction	Site	E_{ads} (eV)	Distance (Å)
SnO_2(100)(I)/CoO(110)(II)	O_2	−0.2286	2.4615
	O1	−0.6962	3.3761
	O2	−0.3900	4.1691
	Co1	−0.0898	3.1388
	Co2	1.6229	4.3275
CoO(110)(II)/SnO_2(100)(II)	O_2	−0.2957	3.0844
	Sn	−0.3855	3.4432
	O1	−0.2551	3.2475
	O2	−0.2496	3.8159

is shown in Fig. S3 and S4 (ESI†). Then, the effect of H_2 adsorption on the surface conductivity of single metal oxide was studied under oxygen conditions. Finally, the gas-sensing properties of the heterojunction were studied under oxygen conditions.

The adsorption of H_2 in the oxygen atmosphere will affect the heterojunction resistance, which could be reflected in DOS. Therefore, the change in the resistance can be studied by analyzing the DOS. The generation of more peaks and increase in the DOS values were found over the tested energy range, which were attributed to the gas adsorption. The variations in DOS would further account for the increase in the electron energy and the better conductivity.[72–76]

The DOS values for H_2 on the different sites of the SnO_2(100)(I)/CoO(110)(II) and CoO(110)(II)/SnO_2(100)(II) heterojunction surfaces are shown in Fig. 5(a) and (b). In addition, the DOS for H_2 adsorbed on different sites of single metal oxides CoO and SnO_2 are shown in Fig. S5(a) and (b) (ESI†).

Fig. 5(a) shows the DOS for H_2 adsorption on different sites of the SnO_2(100)(I)/CoO(110)(II) heterojunction surface. The DOS value was reduced when H_2 was adsorbed on an O site of the O_2 molecule, labeled as 1 and 2, revealing the heterojunction resistance had increased. The DOS value showed obvious decreases (labeled as 3, 4, and 5) when H_2 was adsorbed on the O1 site, indicating the heterojunction resistance increased along with the adsorption of H_2. When H_2 was adsorbed on the O2 site, a decrease and disappearance of DOS peaks (labeled as 6, 7, and 8) were observed. All these results prove that the resistance increased when H_2 was adsorbed on the O2 site of the heterojunction surface. The DOS value was lower and some peaks disappeared (labeled as 9 and 10) with H_2 adsorbed on the Co1 site, reflecting that the heterojunction resistance had increased. When H_2 was adsorbed on the Co2 site, the changes in the DOS occurred at the Fermi level (labeled as 11, 12, and 13). The DOS value was then reduced and some peaks disappeared, revealing that the heterojunction resistance had increased. On the whole, when H_2 was adsorbed on different sites of the heterojunction surface, the heterojunction resistance increased. Compared with the DOS of the metal oxide CoO (Fig. S5(a), ESI†), the DOS value of the

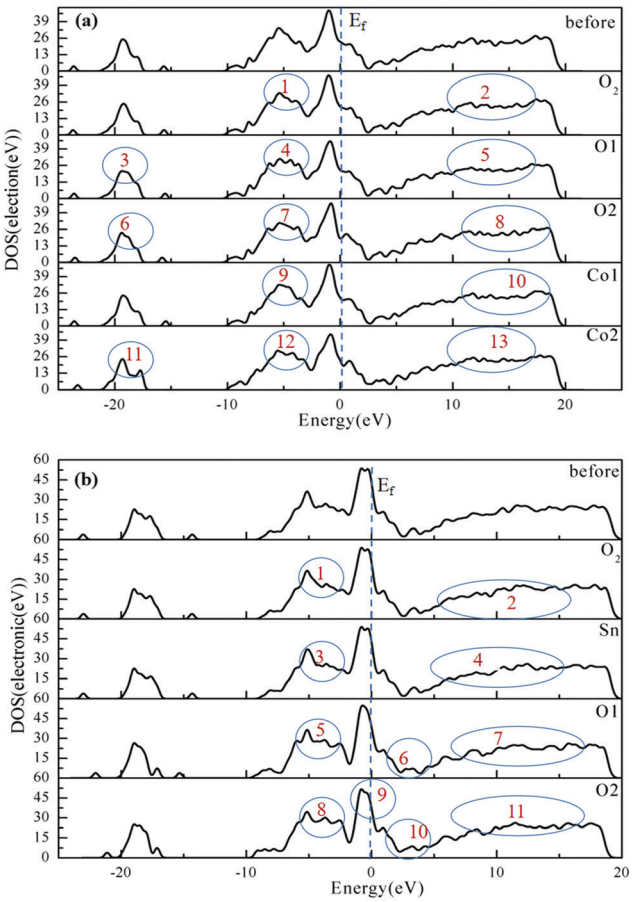

Fig. 5 DOS of H_2 adsorption on different sites of the heterojunction surface. (a) H_2 on O_2 molecule, and O1 site, O2 site, Co1 site, Co2 site of the SnO_2(100)(I)/CoO(110)(II) heterojunction. (b) H_2 on O_2 molecule, and O1 site, O2 site, Sn site of the CoO(110)(II)/SnO_2(100)(II) heterojunction.

SnO_2(100)(I)/CoO(110)(II) heterojunction decreases more obviously. Therefore, the heterojunction changed the gas adsorption performance for H_2.

Fig. 5(b) shows the DOS of H_2 adsorption on different sites of the CoO(110)(II)/SnO_2(100)(II) heterojunction surface. With the adsorption of H_2 on an O_2 molecule, the DOS value was reduced distinctly (labeled as 1 and 2), implying the heterojunction resistance had improved. The DOS showed a slight alteration when H_2 was adsorbed on the Sn site, indicated that the resistance of the heterojunction had slightly changed, together with the disappearance of peaks in the conduction band (labeled as 3 and 4), indicating that the heterojunction resistance was enlarged. In the DOS, the number of peaks disappeared or reduced (labeled as 5, 6, and 7) when H_2 was adsorbed on the O1 site, indicating that the heterojunction resistance had increased. DOS showed a slight reduction and some peaks disappeared (labeled as 8, 9, 10, and 11) when H_2 was adsorbed on the O2 site, indicating that the heterojunction resistance had increased. These results proved the heterojunction resistance increased with the adsorption of H_2. The DOS changes of H_2 on the heterojunction surface was opposite to that for H_2 on the SnO_2 surface (Fig. S5(b), ESI†). This shows that the presence of a heterojunction will change the response trend of H_2 on the SnO_2 surface.

In summary, compared with single metal oxides CoO and SnO_2, the existence of the SnO_2(100)(I)/CoO(110)(II) heterojunction and CoO(110)(II)/SnO_2(100)(II) heterojunction changed the adsorption performance to H_2. The response trend of the SnO_2(100)(I)/CoO(110)(II) heterojunction to H_2 was the same as that with CoO, but the response trend of the CoO(110)(II)/SnO_2(100)(II) heterojunction to H_2 was the opposite as that with SnO_2. This will provide theoretical guidance for the accurate identification of H_2 and the manufacture of sensors.

3.2.2 Electronic structure of H_2 on the SnO_2(100)/CoO(110) heterojunction surface. In order to understand the essence of adsorption, the electronic structure of H_2 adsorption on the SnO_2(100)/CoO(110) heterojunction in an oxygen atmosphere was assessed. The binding of atoms has a strong relationship with the electronic structure, which can be characterized by the electronic density and electronic density difference. The total electronic density and electronic density difference were calculated, and are shown in Fig. 6 and 7, respectively.

Fig. 6 displays the optimized structure, electronic density, and electronic density difference of H_2 adsorption on different sites (including O_2 molecule, O1 site, O2 site, Co1 site and Co2 site) of the SnO_2(100)(I)/CoO(110)(II) heterojunction surface. The optimized structure of H_2 adsorption on an O_2 molecule of the SnO_2(100)(I)/CoO(110)(II) heterojunction surface is shown in Fig. 6(a). The adsorbed distance was 2.4615 Å and E_{ads} was −0.2286 eV, as shown in Table 2. The adsorbed distance was smaller than that for H_2 on other sites of the heterojunction surface.

The blue ranges represent the depletion areas of the electrons, and the red areas show the accumulation region of the electrons. As displayed in Fig. 6(a), H_2 was adsorbed on the O_2 molecule of the heterojunction surface. The adsorbed distance was less than 3 Å and E_{ads} was negative, and the electronic sharing occurred between H atoms and the O_2 molecule. Therefore, the H atoms share an extensive amount of electrons with the O_2 molecule, which indicates that H–O bonding has stronger covalence. In addition, the O_2 molecule shares extensive electrons with atoms of the heterojunction surface, illustrating the stable adsorption of the O_2 molecule on the heterojunction surface and the formation of a covalent bond with atoms of the heterojunction surface. As shown in Fig. 6(a), the H_2 molecule and O_2 molecule, which are adsorbed on the heterojunction surface, get an amount of electrons simultaneously. This implies the existence of an electronic transformation and chemical reaction between H atoms and O atoms of O_2.

The electron sharing hardly occurred and the adsorption distance was greater than 3 Å when H_2 was adsorbed on other sites of the heterojunction surface, and although there was slight electron transfer between the sites, there was no bonding. Therefore, O_2 molecule was the best adsorption site of H_2 on the heterojunction surface and the heterojunction was the best carrier of H_2. In the air environment, the adsorbed O_2

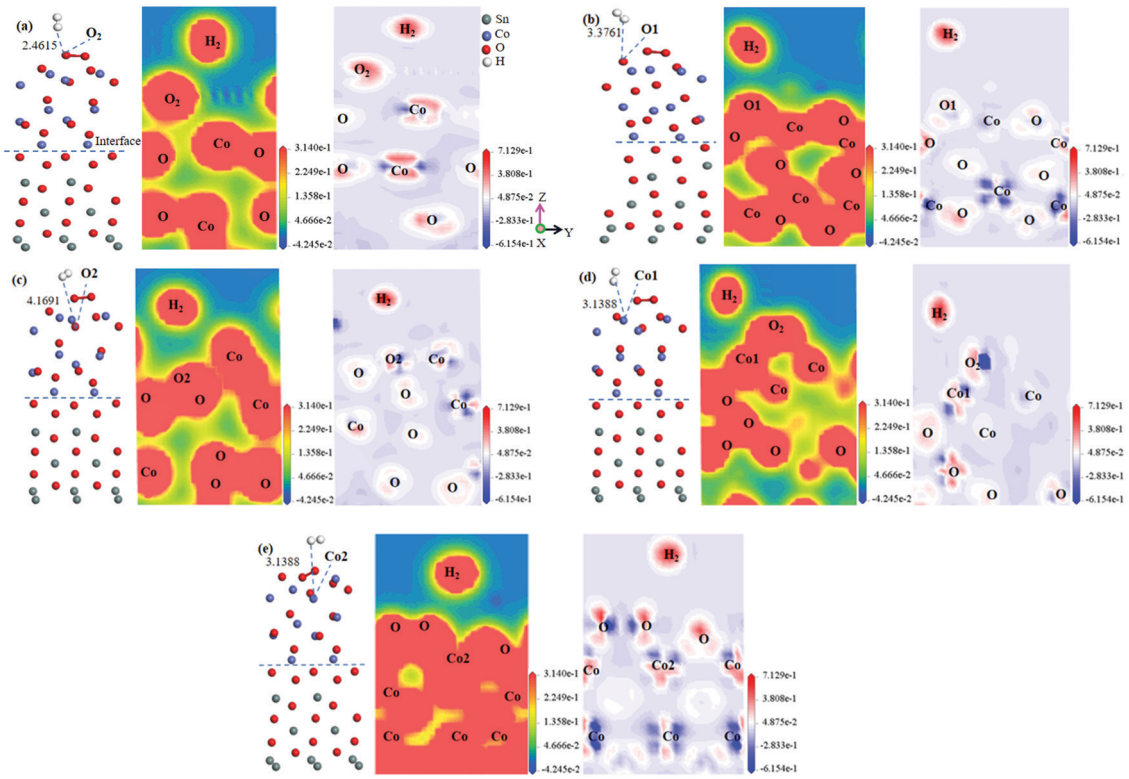

Fig. 6 Electronic structure of H_2 adsorption on different sites of the SnO_2(100)(I)/CoO(110)(II) heterojunction surface. Optimized structure of the heterojunction; electronic density; electronic density difference. (a) H_2 on O_2 molecule, (b) H_2 on O1 site, (c) H_2 on O2 site, (d) H_2 on Co1 site, (e) H_2 on Co2 site.

molecules extract electrons bands of the heterojunction and convert to oxygen species, such as O^{2-}, O^-, and O_2^-, covering the surface of the heterojunction.[77,78] The subsequent reaction ($H_2 + O^{x-} \rightarrow H_2O + xe^-$) releases electrons back into the heterojunction surface.[54] An atomic level understanding of the H_2-sensing mechanism on the heterojunction was thus proved.

3.2.3 Electronic structure of H_2 on the CoO(110)(II)/SnO_2(100)(II) heterojunction. The electronic structures of H_2 adsorption on different sites of the CoO(110)(II)/SnO_2(100)(II) heterojunction surface are shown in Fig. 7, together with the optimized structure of H_2 adsorption on different sites of the heterojunction. The E_{ads} values were all negative when H_2 was adsorbed on different sites of the heterojunction surface. This shows that H_2 can be stably adsorbed on the heterojunction surface.

Fig. 7(a) reveals the electronic density when H_2 was adsorbed on the O_2 molecule. As shown, there was little electronic accumulation between the H atoms and O_2 molecule when H_2 was adsorbed on the O_2 molecule. The H atoms shared a bit of electronic density with the O_2 molecule on the heterojunction surface and the adsorbed distance was more than 3 Å, indicating the existence of a slight H–O covalent bond. Fig. 7(a) shows the electronic density difference when H_2 was adsorbed on the O_2 molecule of the heterojunction surface, whereby the H atoms acquired extensive electrons, and at the same time, a gain and loss of electrons occurred on the O_2 molecule. Consequently, the transformation of the electronic density and the chemical reaction between H atoms and the O_2 molecule were proved. Fig. 7(b) reveals the electronic density when H_2 was adsorbed on the O1 atom of the CoO(110)(II)/SnO_2(100)(II) heterojunction surface. There was clear electronic accumulation between H atoms and the O1 atom when H_2 was adsorbed on the O1 atom. The H atoms shared some electrons with the O1 atom on the SnO_2 side and the adsorbed distance was more than 3 Å, which suggests the existence of H–O bonding. Fig. 7(b) shows the electronic density difference when H_2 was adsorbed on the O1 site of the heterojunction surface; whereby the H atoms acquired some electrons and the O1 atom of the heterojunction surface obtained some electrons too. Consequently, the slight transformation of the electronic density and a slight reaction between the H atoms and O1 atom were proved.

Fig. 7(c) and (d) show the electronic structure when H_2 was adsorbed on the O2 site and Sn site of the heterojunction surface. Barely any electrons existed between H atoms and the O2 atom and Sn atom of the heterojunction surface. This indicated the formation of weaker H–O bonding and H-Sn bonding for H atoms sharing a few electrons with the O2 atom of the heterojunction surface. This means a small transformation in the electronic density and a slight reaction between H_2 and the O1 atom and Sn atom. In summary, O_2 molecule on the heterojunction was the best site for reacting with H_2, and the O1 site was the best adsorption site for H_2.

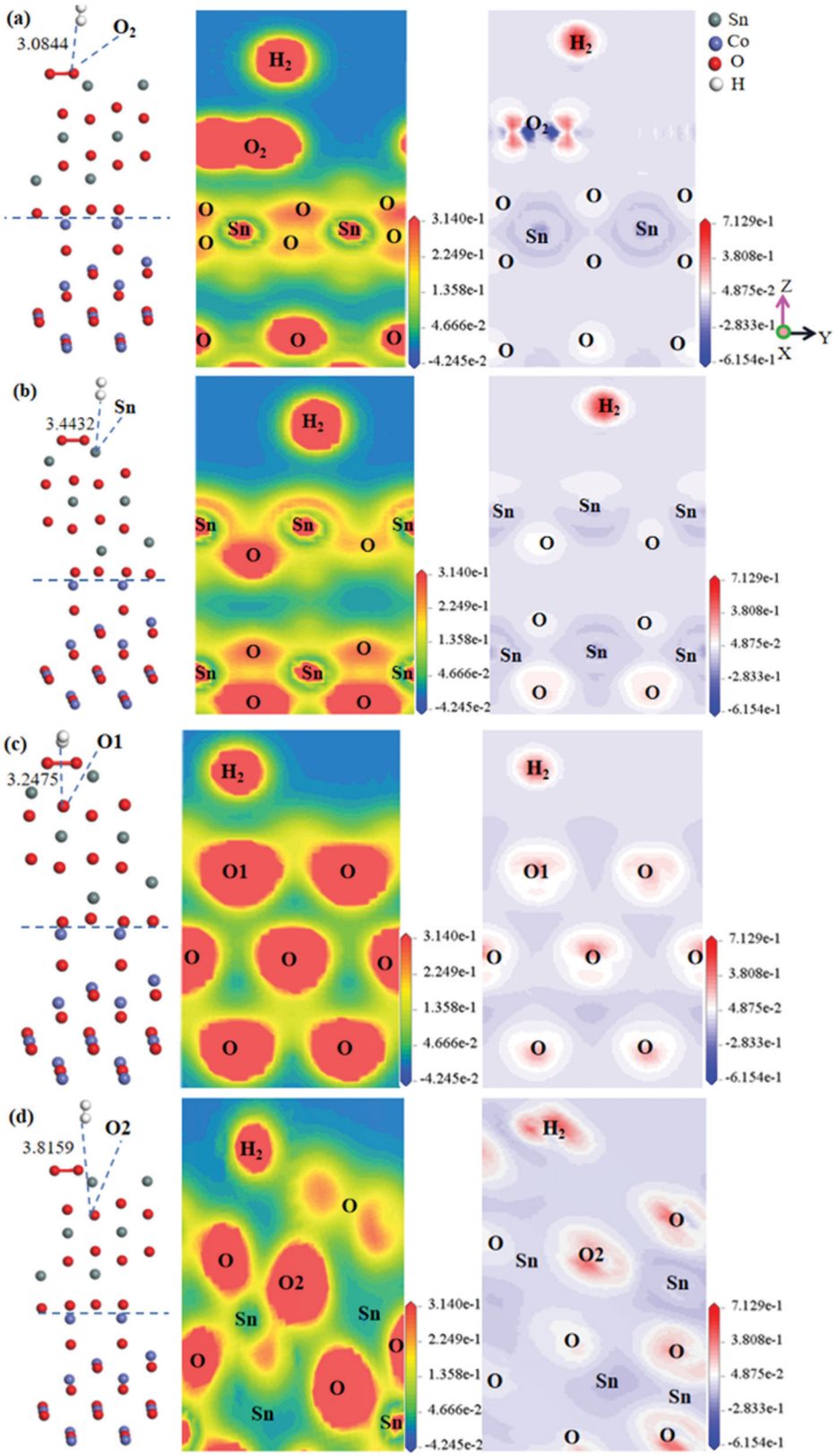

Fig. 7 Electronic structure of H_2 adsorption on different sites of the CoO(110)(II)/SnO_2(100)(II) heterojunction surface. Optimized structure of the heterojunction; electronic density; electronic density difference. (a) H_2 on O_2 molecule, (b) H_2 on O1 site, (c) H_2 on O2 site, (d) H_2 on Sn site.

4. Conclusion

In this study, DFT was used to calculate the adsorption properties of H_2 on CoO/SnO_2 and SnO_2/CoO heterojunction surfaces under air conditions. First, the optimal heterojunction structure was determined based on the W_{ad}. Second, the most stable adsorption configuration of H_2 in the air was identified based on the results of the E_{ads} calculation. Finally, the mechanism of the gas adsorption process was revealed by DOS and by the electronic structure, and the following conclusions were obtained:

(1) A smaller lattice mismatch and larger W_{ad} are associated with a more stable interface. The CoO(110) surface and SnO_2(100) surface were chosen for forming the structure of the heterojunction. SnO_2(100)(I)/CoO(110)(II) and CoO(110)(II)/SnO_2(100)(II) were more stable than other SnO_2(100)/CoO(110) and CoO(110)/SnO_2(100) heterojunctions. Therefore, the stability, resistance, and electronic structure of SnO_2(100)(I)/CoO(110)(II) and CoO(110)(II)/SnO_2(100)(II) heterojunctions were mainly studied as carriers of H_2 in oxygen atmosphere.

(2) The heterojunction resistance increased when H_2 was adsorbed on different sites of the SnO_2(100)(I)/CoO(110)(II) surface, which, followed the same trend as for H_2 adsorption on the CoO surface. Moreover, its trend of change was greater according to DOS. This shows that the heterojunction can change the gas adsorption performance of H_2. The O_2 molecule on the heterojunction surface is the best adsorption site for H_2, because of the larger electron density distribution between them. In addition, the heterojunction is the best carrier of H_2 for the existence of the reaction between H_2 and surface oxygen ions. An atomic level understanding of the H_2 sensing mechanism on the heterojunction was proved.

(3) The heterojunction resistance increased when H_2 was adsorbed on different sites of the CoO(110)(II)/SnO_2(100)(II) surface. Also, the heterojunction resistance showed the opposite trend to H_2 adsorption on the SnO_2 surface. When the SnO_2/CoO heterojunction was exposed to H_2 gas, H_2 reacted with the oxygen ions on the SnO_2 surface and the electrons returned to the conduction band, which led to energy band bending. Nonetheless, H_2 hardly reacted with the oxygen ions on the CoO surface. As a result, the potential barrier of SnO_2/CoO increased, leading to an increase in resistance and a p-type response to H_2. Therefore, the presence of the heterojunction will change the trend of the response to H_2. Meanwhile, according to the electronic density, the O1 site of the heterojunction surface was the best adsorption site for H_2, because of the larger electron density distribution among them. Finally, as judged by E_{ads}, the heterojunction improved the stability of H_2 adsorption on the surface.

Conflicts of interest

There are no conflicts declare.

Acknowledgements

We are very grateful for the support of the National Natural Science Foundation of China (Fund number: 51974157, 51874169, 51774180 and 51634004).

References

1 C. B. Lim and S. Oh, Microstructure evolution and gas sensitivities of Pd-doped SnO_2-based sensor prepared by three different catalyst-addition processes, *Sens. Actuators, B*, 1996, **30**, 223–231.
2 F. Hartmann, Semiconductor sensors, *Nucl. Instrum. Methods Phys. Res*, 2011, **628**, 40–49.
3 A. T. Güntner and N. J. Pineau, *et al.*, Sniffing Entrapped Humans with Sensor Arrays, *Anal. Chem.*, 2018, **90**, 4940–4945.
4 M. Righettoni, A. Amann and E. S. Pratsinis, Breath analysis by nanostructured metal oxides as chemo-resistive gas sensors, *Mater. Today*, 2015, **18**, 163–171.
5 P. Reimann, A. Dausend and A. Schutze, A self-monitoring and self-diagnosis strategy for semiconductor gas sensor systems, *SENSORS, 2008 IEEE*, 2008, 192–195.
6 M. Schüler, T. Sauerwald and A. Schütze, A novel approach for detecting HMDSO poisoning of metal oxide gas sensors and improving their stability by temperature cycled operation, *J. Sens. Sens. Syst.*, 2015, **4**, 305–311.
7 L. P. Huo, Y. Xi and Z. Liu, *et al.*, Modulation of Potential Barrier Heights in Co_3O_4/SnO_2 Heterojunction for Highly H_2-Selective Sensors, *Sens. Actuators, B*, 2017, **244**, 694–700.
8 N. V. Toan and N. V. Duy, *et al.*, Fabrication of highly sensitive and selective H_2 gas sensor based on SnO_2 thin film sensitized with microsized Pd islands, *J. Hazard. Mater.*, 2015, **301**, 433–442.
9 C. Liewhiran, N. Tamaekong and A. Wisitsoraat, *et al.*, Ultrasensitive H_2 sensors based on flame-spray-made Pd-loaded SnO_2 sensing films, *Sens. Actuators, B*, 2013, **176**, 893–905.
10 C. B. Lim and S. Oh, Microstructure evolution and gas sensitivities of Pd-doped SnO_2-based sensor prepared by three different catalyst-addition processes, *Sens. Actuators, B*, 1996, **30**, 223–231.
11 F. D. Manchester, A. San-Martin and J. M. Pitre, The H-Pd (hydrogen-palladium) System, *J. Phase Equilib.*, 1994, **15**, 62–83.
12 G. Lu and J. T. Hupp, Metal–organic frameworks as sensors: a ZIF-8 based Fabry-Pérot device as a selective sensor for chemical vapors and gases, *J. Am. Chem. Soc.*, 2010, **132**, 7832–7833.
13 M. Drobek, J. H. Kim and M. Bechelany, *et al.*, MOF-Based Membrane Encapsulated ZnO Nanowires for Enhanced Gas Sensor Selectivity, *ACS Appl. Mater. Interfaces*, 2016, **8**, 8323–8328.
14 H. Tian, H. Fan and M. Li, *et al.*, Zeolitic Imidazolate Framework Coated ZnO Nanorods as Molecular Sieving to Improve Selectivity of Formaldehyde Gas Sensor, *ACS Sens.*, 2016, **1**, 243–250.
15 M. S. Yao and W. Xiang, *et al.*, MOF Thin Film-Coated Metal Oxide Nanowire Array: Significantly Improved Chemiresistor Sensor Performance, *Adv. Mater.*, 2016, **28**, 5229–5234.
16 J. Hong, S. Lee, J. Seo, S. Pyo, J. Kim and T. Lee, A highly sensitive hydrogen sensor with gas selectivity using a PMMA membrane-coated Pd nanoparticle/single-layer graphene hybrid, *ACS Appl. Mater. Interfaces*, 2015, **7**, 3554–3561.

17 O. Lupan, V. Postica and J. Ttrup, *et al.*, Hybridization of Zinc Oxide Tetrapods for Selective Gas Sensing Applications, *ACS Appl. Mater. Interfaces*, 2017, **9**, 4084–4099.
18 V. Musat, E. Fortunato and A. M. Botelho do Rego, *et al.*, Sol-gel cobalt oxide-silica nanocomposite thin films for gas sensing applications, *Thin Solid Films*, 2008, **516**, 1499–1502.
19 M. Matsumiya, F. Qiu and W. Shin, *et al.*, Thermoelectric CO Gas Sensor Using Thin-Film Catalyst of Au and Co_3O_4, *J. Electrochem. Soc.*, 2003, **151**, H7.
20 Q. Jiao, M. Fu and C. You, *et al.*, Preparation of hollow Co_3O_4 microspheres and their ethanol sensing properties, *Inorg. Chem.*, 2012, **51**, 11513–11520.
21 X. Yu, X. Liu and M. Wu, *et al.*, Hierarchical radial Co_3O_4 microcrystal and application in gas sensor, *Chin. J. Chem. Phys.*, 2014, **27**, 99–102.
22 D. Barreca, E. Comini and A. P. Ferrucci, *et al.*, First Example of ZnO-TiO_2 Nanocomposites by Chemical Vapor Deposition: Structure, Morphology, Composition, and Gas Sensing Performances, *Chem. Mater.*, 2007, **19**, 5642–5649.
23 W. J. Moon, H. J. Yu and G. M. Choi, The CO and H_2 gas selectivity of CuO-doped SnO_2–ZnO composite gas sensors, *Sens. Actuators, B*, 2002, **87**, 464–470.
24 J. H. Kim, J. H. Lee and A. Mirzaei, *et al.*, SnO_2 (n)-NiO (p) composite nanowebs: gas sensing properties and sensing mechanisms, *Sens. Actuators, B*, 2017, **258**, 204–214.
25 D. R. Miller, S. A. Akbar and P. A. Morris, Nanoscale metal oxide-based heterojunction for gas sensing: a review, *Sens. Actuators, B*, 2014, **204**, 250–272.
26 Y. Liu, G. Li and R. Mi, *et al.*, An environment-benign method for the synthesis of p-NiO/n-ZnO heterostructure with excellent performance for gas sensing and photocatalysis, *Sens. Actuators, B*, 2014, **191**, 537–544.
27 J. Martinez, S. B. Sinnott and S. R. Phillpot, Adhesion and diffusion at TiN/TiO_2 interfaces: a first principles study, *Comput. Mater. Sci.*, 2017, **130**, 249–256.
28 J. H. Kim, J. H. Lee and A. Mirzaei, *et al.*, SnO_2(n)-NiO(p) composite nanowebs: gas sensing properties and sensing mechanisms, *Sens. Actuators, B*, 2017, **258**, 204–214.
29 B. Xu, C. Zhu and X. He, *et al.*, First-Principles Calculations on Atomic and Electronic Properties of Ge/4H-SiC Heterojunction, *Adv. Conden. Matter Phys.*, 2018, **3**, 1–9.
30 X. Fan, B. Chen and M. Zhang, *et al.*, First-principles calculations on bonding characteristic and electronic property of TiC(111)/TiN(111) interface, *Mater. Des.*, 2016, **112**, 282–289.
31 A. Katoch, S. W. Choi and J. H. Kim, *et al.*, Importance of the nanograin size on the H_2S-sensing properties of ZnO–CuO composite nanofibers, *Sens. Actuators, B*, 2015, **214**, 111–116.
32 S. W. Choi, Z. Jin and K. Akash, *et al.*, H_2S sensing performance of electrospun CuO-loaded SnO_2 nanofibers, *Sens. Actuators, B*, 2012, **169**, 54–60.
33 D. Ju, H. Xu and Q. Xu, *et al.*, High triethylamine-sensing properties of NiO/SnO_2 hollow sphere P–N heterojunction sensors, *Sens. Actuators, B*, 2015, **215**, 39–44.
34 Q. Zhi, Y. Fu and B. Yu, *et al.*, High and fast H_2S response of NiO/ZnO nanowire nanogenerator as a self-powered gas sensor, *Sens. Actuators, B*, 2016, **222**, 78–86.
35 Y. T. Kwon and W. H. Yeo, Flexible, Wearable, and Stretchable Electronics, Flexible, Wearable, and Stretchable Electronics, 2020, 1–30.
36 J. J. Kim, S. J. Chung and J. W. Choi, *et al.*, Redox Reaction between Nitric Oxide and Carbon Monoxide over Perovskite-type Catalysts, *J. Korean Inst. Chem. Eng.*, 1982, **20**, 245.
37 L. Wang, J. Deng and Z. Lou, *et al.*, Cross-linked p-type Co_3O_4 octahedral nanoparticles in 1D n-type TiO_2 nanofibers for high-performance sensing devices, *J. Mater. Chem. A*, 2014, **2**, 10022–10028.
38 X. T. Yin, J. Li and D. Dastan, *et al.*, Ultra-high selectivity of H_2 over CO with a p–n nanojunction based gas sensors and its mechanism, *Sens. Actuators, B*, 2020, **319**, 128330.
39 B. L. Bramfitt, The effect of carbide and nitride additions on the heterogeneous nucleation behavior of liquid iron, *Metall. Trans.*, 1970, **1**, 1987–1995.
40 H. Zhang and H. Xiong, First-principles study of NbC heterogeneous nucleation on TiC *vs.* TiN in microalloy steel, *Ironmaking Steelmaking*, 2018, **47**, 77–83.
41 A. Mirzaei, S. G. Leonardi and G. Neri, Detection of hazardous volatile organic compounds (VOCs) by metal oxide nanostructures-based gas sensors: a review, *Ceram. Int.*, 2016, **42**, 15119–15141.
42 Y. Jian, J. Huang and D. Fan, *et al.*, First-principles investigation on the electronic property and bonding configuration of NbC(111)/NbN(111) interface, *J. Alloys Compd.*, 2016, **689**, 874–884.
43 X. Fan, B. Chen and M. Zhang, *et al.*, First-principles calculations on bonding characteristic and electronic property of TiC(111)/TiN(111) interface, *Mater. Des.*, 2016, **112**, 282–289.
44 L. Shi, H. Yan and Z. H. Lu, *et al.*, Surface Property of the Cu Doped γ-Al_2O_3: A Density Functional Theory Study, *Appl. Surf. Sci.*, 2020, **535**, 147651.
45 G. Feng, Q. Xiao and D. S. Wang, *et al.*, Acid properties of Ni-modified ZSM-12: a first-principles Study, *J. Fuel Chem. Technol.*, 2020, **48**, 704–712.
46 G. Feng, J. Yang and C. Wang, *et al.*, A first-principles study on Pd modified ZSM-12 zeolites, *Microporous Mesoporous Mater.*, 2018, **260**, 227–234.
47 G. Feng, M. V. Ganduglia-Pirovano and C. F. Huo, *et al.*, Hydrogen spillover to copper clusters on hydroxylated γ-Al_2O_3, *J. Phys. Chem. C*, 2018, **122**, 18445–18455.
48 X. Yu, X. Zhang and H. Wang, *et al.*, High-coverage H_2 adsorption on the reconstructed Cu_2O(111) surface, *J. Phys. Chem. C*, 2017, **121**, 22081–22091.
49 L. Shi, S. Meng and S. Jungsuttiwong, *et al.*, High coverage H_2O adsorption on $CuAl_2O_4$ surface: a DFT study, *Appl. Surf. Sci.*, 2020, **507**, 145162.
50 L. Ou, Y. Fan and Y. Liu, *et al.*, First-Principle Study of the Adsorption and Dissociation of O_2 on Pt(111) in Acidic Media, *J. Phys. Chem. C*, 2009, **113**, 20657–20665.

51 J. Chen and C. Ye, A first-principle study of the effect of vacancy defects and impurities on the adsorption of O_2 on sphalerite surfaces – Science Direct, *Colloids Surf., A*, 2010, **363**, 56–63.
52 H. Xiong and Z. Liu, *et al.*, First principles calculation of interfacial stability, energy and electronic properties of SiC/ZrB_2 interface-Science Direct, *J. Phys. Chem. Solids*, 2017, **107**, 162–169.
53 Y. Jian, J. Huang and D. Fan, *et al.*, First-principles investigation on the electronic property and bonding configuration of NbC(111)/NbN(111) interface, *J. Alloys Compd.*, 2016, **689**, 874–884.
54 W. H. Lee and X. H. Yao, First principle investigation of phase transition and thermodynamic properties of SiC, *Comput. Mater. Sci.*, 2015, **106**, 76–82.
55 L. Huo, Y. Xi and Z. Liu, *et al.*, Modulation of Potential Barrier Heights in Co_3O_4/SnO_2 Heterojunction for Highly H_2-Selective Sensors, *Sens. Actuators, B*, 2017, **244**, 694–700.
56 B. L. Bramfitt, The effect of carbide and nitride additions on the heterogeneous nucleation behavior of liquid iron, *Metall. Trans.*, 1970, **1**, 1987–1995.
57 H. Zhang and H. Xiong, First-principles study of NbC heterogeneous nucleation on TiC *vs*., TiN in microalloy steel, *Ironmaking Steelmaking*, 2018, **47**, 77–83.
58 R. Liu, X. Yin and K. Feng, *et al.*, First-principles calculations on Mg/TiB_2 interfaces, *Comput. Mater. Sci.*, 2018, **149**, 373–378.
59 L. Xiao, Q. Hui and D. Shao, *et al.*, First-principles study on the stability and electronic structure of Mg/ZrB_2 interfaces, *Sci. China: Mater.*, 2016, **59**, 28–37.
60 H. H. Xiong, H. N. Zhang and J. H. Dong, Adhesion strength and stability of TiB_2/TiC interface in composite coatings by first principles calculation, *Comput. Mater. Sci.*, 2017, **127**, 244–250.
61 L. Jian, Y. Yang and G. Feng, *et al.*, First-principles study of stability and properties on β-SiC/TiC(111) interface, *J. Appl. Phys.*, 2013, **114**, 54–59.
62 D. Yin, X. Peng and Y. Qin, *et al.*, Electronic property and bonding configuration at the TiN(111)/VN(111) interface, *J. Appl. Phys.*, 2010, **108**, 033714.
63 D. Y. Dang, L. Y. Shi and J. L. Fan, *et al.*, First-principles study of W-TiC interface cohesion, *Surf. Coat. Technol.*, 2015, **276**, 602–605.
64 N. Chandran, M. Sall and J. Arvanitidis, *et al.*, On the formation of graphene by Ge intercalation of a 4H-SiC surface, *Mater. Sci. Forum*, 2015, **821**, 961–964.
65 H. Zhang and H. Xiong, First-principles study of NbC heterogeneous nucleation on TiC *vs*. TiN in microalloy steel, *Ironmaking Steelmaking*, 2018, **47**, 77–83.
66 H. J. Kim and J. H. Lee, Highly sensitive and selective gas sensors using p-type oxide semiconductors: overview, *Sens. Actuators, B*, 2014, **192**, 607–627.
67 S. Chu and A. Majumdar, Opportunities and challenges for a sustainable energy future, *Nature*, 2012, **488**, 294–303.
68 L. Tao, J. Huang and D. Dastan, *et al.*, New insight into absorption characteristics of CO_2 on the surface of calcite, dolomite, and magnesite, *Appl. Surf. Sci.*, 2021, **540**, 148320.
69 L. Tao, J. Huang and D. Dastan, *et al.*, CO_2 capture and separation on charge-modulated calcite, *Appl. Surf. Sci.*, 2020, **530**, 147265.
70 M. Viitala, *et al.*, Conformation and energetics of benzene adsorbate on SnO_2(110) surfaces: a first principles study, *Surf. Sci.*, 2011, **605**, 1563–1567.
71 Z. Wen, T. M. Liu and D. J. Liu, Formaldehyde gas sensing property and mechanism of TiO_2–Ag nanocomposite, *Phys. B*, 2010, **405**, 4235–4239.
72 M. H. Li, H. C. Zhu and G. F. Wei, *et al.*, DFT calculation and analysis of the gas sensing mechanism of methoxy propanol on Ag decorated SnO_2(110) surface, *RSC Adv.*, 2019, **9**, 35862–35871.
73 W. Zeng, T. M. Liu and D. J. Liu, *et al.*, Hydrogen sensing and mechanism of M-doped SnO_2 (M = Cr^{3+}, Cu^{2+} and Pd^{2+}) nanocomposite, *Sens. Actuators, B*, 2011, **160**, 455–462.
74 W. Zeng, T. M. Liu and X. F. Lei, Hydrogen sensing properties of low-index surfaces of SnO_2 from first-principles, *Phys. B*, 2010, **405**, 3458–3462.
75 S. Yang, Z. Lan and H. Xu, *et al.*, A First-Principles Study on Hydrogen Sensing Properties of Pristine and Mo-Doped Graphene, *J. Nanotechnol.*, 2018, **2018**, 1–5.
76 Y. H. Zhang, L. F. Han and Y. H. Xiao, *et al.*, Understanding dopant and defect effect on H_2S sensing performances of graphene: a first-principles study, *Comput. Mater. Sci.*, 2013, **69**, 222–228.
77 A. Gurlo and R. Riedel, In situ and operando spectroscopy for assessing mechanisms of gas sensing, *Angew. Chem., Int. Ed.*, 2007, **46**, 3826–3848.
78 A. Gurlo, Interplay between O_2 and SnO_2: oxygen ionosorption and spectroscopic evidence for adsorbed oxygen, *Phys. Chem. Chem. Phys.*, 2006, **7**, 2041–2052.